**Annales
Geophysicae**

Observations of multi-microsecond VHF pulsetrains in energetic intracloud lightning discharges

A. R. Jacobson[1], R. H. Holzworth[1], and X.-M. Shao[2]

[1]Earth and Space Sciences, University of Washington, P.O. Box 351310, Seattle, WA 98229-1310, USA
[2]Los Alamos National Laboratory, Los Alamos, NM 87545, USA

Abstract. Certain intracloud lightning discharges emit energetic, multi-microsecond pulsetrains of radio noise. Observations of this distinctive form of lightning date from 1980 and have involved both ground-based and satellite-based radio recording systems. The underlying intracloud lightning discharges have been referred to as "Narrow Bipolar Pulses", "Narrow Bipolar Events", and "Compact Intracloud Discharges". An important discriminant for this species of radio emission is that, in the range above ∼30 MHz, it consists of several microseconds of intense radio noise.

When the intracloud emission is viewed from a satellite, each radio pulsetrain is received both from a direct lightning-to-satellite path, and after some delay, from a path via ground. Thus one recording of the radio emission, if of sufficient length, contains the "view" of the intracloud emission from two different angles. One view is of radiation exiting the emitter into the upper hemisphere, the other for radiation exiting into the lower hemisphere. However, the propagation conditions are similar, except that one path includes a ground reflection, while the other does not.

One would normally expect a stereoscopic double view of the "same" emission process to provide two almost congruent time series, one delayed from the other, and also differing due to the different propagation effects along the two signal paths, namely, the ground reflection. We present somewhat unexpected results on this matter, using recordings from the FORTE satellite at a passband 118–141 MHz, with simultaneous data at 26–49 MHz. We find that the 118–141 MHz pulsetrain's detailed time-dependence is completely uncorrelated between the two views of the process. We examine statistics of the 118–141 MHz pulsetrain's integrated power and show that the power emitted into the lower hemisphere, on average, exceeds the power emitted into the upper hemisphere. Finally, we examine statistical measures of the amplitude distribution and show that the 118–141 MHz signal emitted downward is slightly more dominated by discrete, temporally-narrow impulses than is the signal emitted upward.

1 Introduction

The most powerful High Frequency (HF; 3–30 MHz) and Very High Frequency (VHF, 30–300 MHz) emissions from lightning were observed 30 years ago, and were inferred to be due to intracloud discharges (Le Vine, 1980). Le Vine also observed that these HF/VHF bursts occurred simultaneously with "sferics", or Very Low Frequency (VLF, 3–30 kHz)/Low Frequency (LF, 30–300 kHz) radiated electric field pulses from transient charge redistribution (i.e., from current). The accompanying HF noise bursts' duration was several microsec, which was very long compared to the more common leader-step radiation.

The next reported study of these powerful radio pulsetrains (Willett et al., 1989) showed that the HF radiation occurred as an additive, random noise, superimposed on the sferic waveform, rather than as a high-frequency extension of the same spectrum. (See in particular Willett et al's Fig. 2, where the top panel shows the electric-field change, while the lower panel shows the dE/dt that highlights the additive noise.) The authors named these discharges "Narrow Positive (or Negative) Bipolar Pulses", or NPBPs and NNBPs, depending on the sign of the radiated sferic's leading excursion. Henceforth in this paper we will refer to this species of sferic simply as "NBP". Over the next twenty years close variations of this name have been used to reference both the intracloud

Correspondence to: A. R. Jacobson
(abramj@u.washington.edu)

sferic and (somewhat misleadingly) the additive HF/VHF noisy pulsetrain, but these names refer back to the same phenomena described in the 1980s (Le Vine, 1980; Willett et al., 1989). Both of these 1980s studies inferred that the bipolar pulses tended to occur in isolation from more commonly recognized lightning processes, in particular stepped leaders.

This article will present updated observations of the VHF pulsetrains of the sort first identified in the 1980s. We will focus on the pulsetrain time histories, and we will exploit a peculiar feature of lightning-to-satellite observing geometry.

2 Evidence from the Blackbeard receiver on the Alexis satellite

The Blackbeard radio-frequency waveform recorders on the Alexis satellite began in 1993 to provide a different insight (Holden et al., 1995) into the HF/VHF radiation first noted by Le Vine. Blackbeard's triggering was on a simple power threshold, and was therefore quite susceptible to triggering off the noise background. For this reason, Blackbeard was unable to discriminate any but the strongest radio pulses from the quasi-continuous noise background present at the satellite. Thus Blackbeard tended to record almost exclusively those extremely powerful radio bursts first identified by Le Vine. In the satellite view of these noise bursts, each burst occurred as a pair of bursts, separated by tens of microseconds. The observed spectral dispersion was taken as evidence that the pulses had transited the Earth's ionosphere on their path to the satellite, and therefore had originated in the Earth's atmosphere. For this reason, the noise bursts were named "Trans-Ionospheric Pulse Pairs", or TIPPs. These TIPPs tended to occur when the satellite was in view of the known lightning areas such as the Congo Basin, consistent with the noise bursts' association with lightning.

The Blackbeard observations of TIPPs raised the question, what is the physical origin of the doubling of the pulse in a TIPP? One possibility (Rodger, 1999) would be for an intracloud discharge to occur within a thunderstorm, followed by a second discharge in the mesosphere, at the altitude where "sprites" were observed to be initiated. Strong theoretical motivation had already been developed for the second discharge (Roussel-Dupré and Gurevich, 1996; Roussel-Dupre et al., 1994), and shortly thereafter there was observed an instance of HF radar echoes from a mesospheric transient ionization patch over a thunderstorm (Roussel-Dupré and Blanc, 1997). A more prosaic alternative was for the second pulse in the TIPP to be merely a ground reflection of the first pulse.

Blackbeard alone could not resolve this matter, because it could not gather recordings of a series of TIPPs from the same region during the same orbit (Holden et al., 1995). Instead, the TIPP data occurred as single recording that were recovered on the ground only once per satellite-to-ground contact. Had Blackbeard been able to store many TIPPs from the same storm in a single satellite pass within view

of that storm, then the reason for the pulse doubling could have been addressed. The mesospheric hypothesis predicted that the interpulse separation during such a pass would minimize at the highest satellite elevation angles (relative to the storm), and would maximize at the lowest satellite elevation angles. By contrast, the ground-reflection hypothesis predicted precisely the opposite trend. The opportunity to test these predictions on pulse separation was provided by the FORTE satellite (launched in 1997), and the evidence was grossly consistent with the ground-reflection hypothesis (Jacobson et al., 1999). See in particular their Figs. 5–13.

A pair of papers considered in some depth the ground-reflection process in terms of Blackbeard observations (Massey and Holden, 1995; Massey et al., 1998a), referred to below as "MH" and "MHS". (MH and MHS were written before the new evidence from FORTE, so fortunately the authors provided a critical examination of the reflection hypothesis.)

MH used data in which the Blackbeard receiver's useful passband was ~25 to 75 MHz, corresponding to wavelength band of 12 to 4 m. The implied band of radian wavelengths was therefore only ~2 to <1 m. Thus, for the reflection to be specular, logically it would be necessary for the reflecting surface to have an optical figure on the order of 1 m, presumably over the dimension of the Fresnel zone. MH pointed out that it would not be straightforward to find such a smooth reflector, except for a reasonably calm water surface.

Could, then, the reflected pulse be due to a rough (Lambertian) reflector? If that were the case, then the second pulse would systematically be wider than the first pulse, due to the differential travel times for different facets within the Lambertian reflector. The net upshot would be that the second pulse would need to be a few to several microsec wider than the first pulse, especially at low satellite elevation angle, and less so for the unlikely circumstance of satellite at zenith. MH checked this against statistical data from Blackbeard. The recorded pulses' durations were examined, and MH's Fig. 7 showed a histogram of the ratio of the duration of the second pulse to that of the first pulse in the pair. Excluding a few outliers, the ratio peaked near unity and varied only within the range 0.7 to 1.3. Given that the first pulse's duration was typically 4 to 5 µs, it followed that the second pulse's duration exceed the first by only ~1 to 1.5 µs. MH therefore assumed specular reflection: "The data are internally consistent with this assumption, but we are troubled by the apparent implication of very small rms surface height fluctuations."

MHS extended MH's consideration of ground reflection in several important ways. The first extension was to use Blackbeard recordings in an effective passband of 117 to 166 MHz, or a wavelength band of ~2.5 to 1.8 m, i.e., radian wavelengths ~0.4 to 0.3 m. If the reflection were significantly influenced by rough-surface effects, then this change of wavelength compared to MH would have noticeably increased the role of Lambertian scattering and thus the pulse-duration ratio. However, MHS's Fig. 4 shows that this emphatically

does not occur. Therefore MHS concluded that the reflection was primarily specular, even for the reduced wavelengths involved. The second new contribution by MHS was to measure the effective reflectivity of dry, flat ground at a frequency passband near 100 MHz. This was done with an Electromagnetic Pulse (EMP) generator flown on a balloon payload 2.6 km above the ground in the White Sands Missile Range. Receivers on towers about 20 m above the ground were able to record both the incident and the reflected pulses from the EMP generator, while the balloon was at 23-deg elevation angle. MHS found the energy reflection coefficient to be 0.94 ± 0.06 for horizontal polarization and 0.78 ± 0.09 for vertical polarization. The soil at White Sands was characterized as dry and alkaline. They concluded from this balloon experiment that the second pulse in Blackbeard TIPPs could feasibly be a ground reflection.

3 Existing evidence on VHF ground reflection from the FORTE satellite

The FORTE satellite (Jacobson et al., 1999) was launched on 27 August 1997 into a nearly circular orbit at 800 km altitude, with inclination 70 deg. The satellite carried a suite of optical and radio instruments. The study cited here used, and will continue to use, data from the dual-channel radio receiver having 25-MHz bandwidth, whose center could be tuned anywhere in the VHF. For most of the work reported here, the observation mode involved a low band (26 to 51 MHz, henceforth called the "38-MHz band"), and a simultaneous high band (118–143 MHz, henceforth called the "130-MHz band"). The digitization was 50 megasamples/s and 12 bits. The 25-MHz-wide Nyquist passband was prefiltered to approximately 22 or 23 MHz width, by an analog low-pass filter attenuating the uppermost 3 MHz. The trigger was a new multi-channel-coincidence system that simultaneously sampled the transient power on eight different subbands and required, for these studies, that 5 out of the eight subbands be triggered within 160 µs of each other, for a master trigger to be issued. This multi-channel-coincidence system effectively overcame the problems of false triggers from anthropogenic carriers transmissions, and FORTE could be used for studying far weaker radio emissions than could Blackbeard. In fact, the majority of intracloud-VHF recordings were from leader steps, which produce a very weak emission compared to the broader emissions noted by Le Vine. The on-board memory could store up to a couple of thousand lightning-transient recordings, each two channels, with 400-µs duration each. The satellite could downlink data several times per day, resulting in up to several-thousand VHF recordings per day. The antenna was a crossed-pair, dual-polarization log-periodic on a 10-m boom directed at nadir. Each of the VHF receivers described above could be connected with either of the crossed antennas.

Details on the FORTE radio system and its performance are available elsewhere (Jacobson et al., 1999; Jacobson and Shao, 2001, 2002a; Jacobson, 2003a, b; Jacobson and Light, 2003; Light et al., 2001; Light and Jacobson, 2002; Shao et al., 2004; Shao and Jacobson, 2001, 2002).

The capability of FORTE's radio payload was soon applied to, among other things, the problem of what accounts for the second pulse in TIPPs. As already mentioned, the FORTE team encountered overwhelming evidence that the second pulse in a TIPP had to be a signal reflected from the ground (Jacobson et al., 1999). The ratio of the energy in the second pulse to that in the first pulse of a TIPP was examined and compared to what might be expected from common land and oceanic reflecting surfaces (Tierney et al., 2002). This study (subsequently "T2002") used the 38-MHz band, and identified 2467 geolocated VHF TIPPs, including 481 over land, 1038 over sea, and 948 over "coastal regions", that is, close enough to both land and sea to be uncertain between the two, within the geolocation accuracy. These TIPPs used by T2002 were not selected to be solely due to intense discharges such as Blackbeard was limited to recording, and in fact the dataset included both intracloud leader-step and isolated intracloud multi-microsecond discharges. T2002 quantified the energy ratio between the received signals in the second versus first pulse of the TIPPs. The average energy ratios observed were 0.39 for land and 0.94 for oceanic lightning. About 25 % of the recordings had a stronger second pulse than first pulse, and most of these 25 % were due to the oceanic and coastal events. T2002 noted that radiation from a linear dipole could produce pulse-energy ratios >1; for example the extreme occurs if the satellite were in line with the dipole axis (the beamlobe's null) and the specular reflection were on the dipole's equator. Finally, T2002 compared the reflectivity averages with expected Fresnel reflection coefficients using best available conductivity and dielectric-constant data. The range of measured and predicted Fresnel pulse-energy ratios were in good agreement, within the uncertainy due to unknown orientation of the radiator dipole axis (or axes).

Thus the existing work on ground reflectivity (Massey and Holden, 1995; Massey et al., 1998a; Tierney et al., 2002) justifies approximating the ground as a specular reflector, with the ocean a more reflective surface (approaching 100 %) than is dry ground.

A different, and in some ways more exigent, test of Earth-surface reflectivity has also been performed. The majority of intracloud radio emissions at 38 MHz are due to leader steps, whose pulse structure is simple and coherent (Jacobson and Light, 2003). That is, the multi-microsecond-duration noise bursts constitute a minority of intracloud emissions seen by FORTE. The more numerous leader steps allow a further test of ground reflectivity: The polarization state of coherent lightning emissions in the 38-MHz band has been measured with the dual, crossed antennas on FORTE (Shao and Jacobson, 2001, 2002). For those intracloud discharges whose first

pulse is polarized, it was found that the second pulse is almost, if not equally, polarized as the first pulse. This could not happen if the ground reflector were substantially Lambertian.

4 Revisiting intracloud VHF pulses with FORTE data: data selection

4.1 Frequency band

Our goal here is to study the time-histories of the multi-microsecond intracloud VHF emissions of the sort originally identified thirty years ago (Le Vine, 1980), and we will exclude the more common leader pulses from this study. By sheer number, most FORTE recordings of intracloud VHF emissions are for coherent, polarized, and narrow pulses. These narrow pulses are seldom solitary; rather, they frequently recur with irregular interpulse separations characteristic of progressive negative leaders (Jacobson and Light, 2003). With diligent effort, in some circumstances with the FORTE low band ("38 MHz") one can remove most of the ionospheric dispersion and also isolate the two birefringent propagation modes from each other (Huang and Roussel-Dupré, 2005, 2006; Jacobson et al., 1999; Jacobson and Shao, 2001, 2002b; Jacobson and Light, 2003; Massey et al., 1998b; Roussel-Dupré et al., 2001). When one succeeds in separating the modes, one can measure the emission pulsewidth of either mode individually. The intrinsic width of each single-mode pulse is typically on the order of $0.05\,\mu s$, although that is an upper bound due to the finite recording bandwidth (22 MHz) and the residual effects of ionospheric dispersion (Roussel-Dupré et al., 2001).

By contrast, the emissions that were recorded by Blackbeard, and originally noted earlier in ground observations (Le Vine, 1980; Willett et al., 1989), have pulsewidths of several microseconds; MHS found about $4\,\mu s$ was typical for the passband 116–166 MHz. Therefore the logical discriminant in separating the wide pulsetrains from the leader pulses is the pulse duration.

During the period October 1997 through September 1998, most dual-receiver FORTE VHF recordings were at both the 38-MHz and the 130-MHz bands simultaneously. The use of pulsewidth to discriminate between the lightning types always works well at 130 MHz, but works less well at 38 MHz. This is primarily because of the birefringent mode splitting. The relative delay between the two modes in most cases scales as the inverse cube of the radio frequency (Massey et al., 1998b; Roussel-Dupré et al., 2001). In the 38-MHz band, the separation can be quite severe (up to $\sim 10\,\mu s$), although it is typically on the order of a couple of microsec, depending on ionospheric conditions and viewing direction relative to the geomagnetic field. This dispersive mode separation by a couple of microsec causes the pulse power envelopes of narrow pulses measured in the 38-MHz band, even after

dechirping the effects of gross dispersion varying as f^{-2}, to be greatly broadened relative to the emitted pulse prior to its transionospheric propagation. However, in the 130-MHz band, the effects of mode splitting are suppressed by the inverse cube of the frequency, so the nominal $2\,\mu s$ of splitting at 38 MHz would imply a splitting at 130 MHz of only $\sim (2\,\mu s) \times (38/130)^3 \sim 0.05\,\mu s$. This is just the bandwidth-limited width anyway. Thus it is best to use the 130-MHz band as the primary tool for determining pulse interior structure, overall pulsewidth, and relationship between the direct signal and the signal arriving via the ground. We shall use the 38-MHz band only for supporting data, as its residual dispersion and mode-splitting blur the features we wish to examine.

4.2 Setting thresholds in signal quality

We will make two data selections. One will have more events, because its selection criteria will be less stringent; the other will have fewer events, because its selection criteria will be more stringent.

The intracloud discharge recordings selected for this study must have the following:

1. Readily identifiable double-pulse form, with a clear separation between the two pulses.

2. Good contrast between the pulse peak and the recordings background noise.

3. Wide pulse structure in the 130-MHz band.

Figure 1a shows the geometry of spacecraft, intracloud lightning, and both the direct path and the path via the reflective ground. Figure 1b shows the square of the electric field at FORTE in the 38-MHz band, averaged over a moving 1-μs window, for a particular 400-μs recording. The signal has already been dechirped and pre-whitened, as explained elsewhere (Jacobson et al., 1999). The double-path structure is clearly visible. The contrast is defined as the ratio of the maximum E^2 to the median E^2. In the study to follow, we will define two sets of data, with 130-MHz contrast ratio >20 (for the less stringent selection) and with contrast >100 (for the more stringent selection.)

Figure 1c shows the lagged autocorrelation of E^2. We will require the central peak's 1/e half-width in the 130-MHz band to exceed $2\,\mu s$. This completely excludes narrow, coherent VHF signals typical of progressing leaders. Requiring the 1/e width >2 μs essentially focuses both of the data sets on the multi-microsec-wide emissions first noted by Le Vine. Figure 1c also shows the lagged peak, at the relative lag of the path via ground relative to the direct path. To ensure ready time separation between the two pulses, we require that the lag be no less than $20\,\mu s$. We characterize the signal-to-noise ratio (SNR) of this lagged peak as its peak amplitude
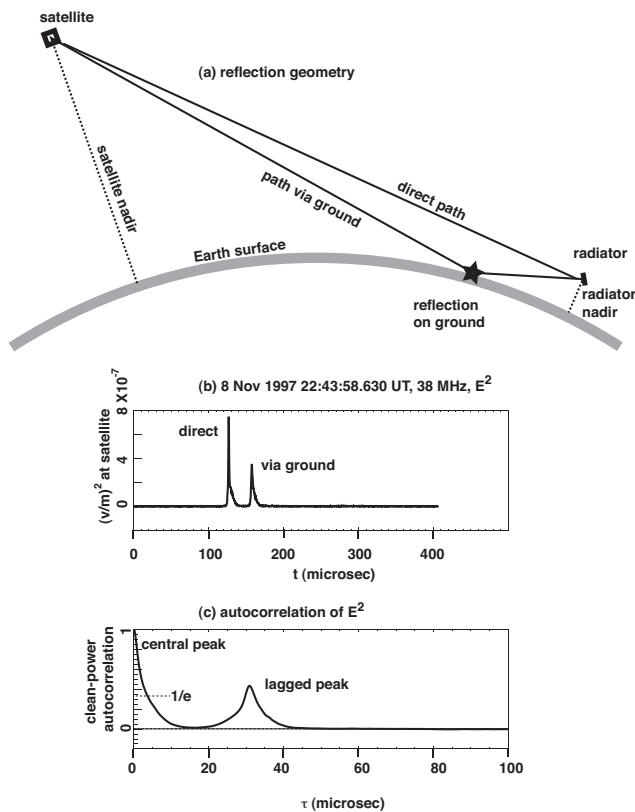
Fig. 1. (a) Scheme of viewing geometry. Lightning above ground is viewed both along a direct path and via the ground, which acts as a good reflector for VHF. **(b)** Sequence of 1-µs-averaged E^2 showing two pulses recorded by FORTE satellite. The signal has been dechirped and "prewhitened", which cleans it of most noise from man-made radio carriers. We define the "contrast" of the signal as the ratio of the maximum E^2 to the median E^2. **(c)** Lagged autocorrelation function of E^2 from this signal. The lagged peak occurs at the interpulse delay. We define the signal-to-noise ratio (snr) of the lagged peak as the peak divided by the root-mean-square residual noise in the correlation at greater lags than the lagged peak.

divided by the rms random fluctuations in the autocorrelation at more than twice the width away from either the central or the lagged peak. We will require that SNR >5 for the less stringent, and >20 for the more stringent data selections. The presence of a ground-reflected pulse following the direct pulse allows inference of the source height (Jacobson et al., 1999).

4.3 Geolocation of the lightning

Lightning emissions were collected but not well geolocated by FORTE's radio instruments alone. More data is needed for geolocation. We geolocate the lightning from three added data sources:

1. coincidence with strokes located by the National Lightning Detection Network (Jacobson et al., 2000);

Table 1. Selected data sets.

Parameter	Less stringent data set	More stringent data set
130-MHz contrast ratio	>20	>100
130-MHz lagged-peak SNR	>5	>20
130-MHz 1-µs-avg ERP	>0.2 kW	>2 kW
130-MHz interpulse separation	>20 µs	>20 µs
130-MHz autocor 1/e width	>2 µs	>2 µs
Number of events in data set	3798	856

2. coincidence with strokes located by the Los Alamos Sferic Array (Smith et al., 2002);

3. coincidence with signals from the optical lightning mapper aboard FORTE (Suszcynsky et al., 2000, 2001).

It is possible in many cases to identify a storm in which some, but not all, of the radio emissions received by FORTE are directly geolocated by the other data sources. In this circumstance, we apply the geolocation to all events in the same storm containing at least three coincidence-located events (Jacobson, 2003a, b; Jacobson and Light, 2003).

For the period in which dual-frequency-band recording was performed (October 1997 through September 1998), the total of geolocated intracloud events (TIPPs) was $> 2 \times 10^4$ recordings. Most of these were narrow, coherent leader steps, but some were multi-microsec emissions. The geolocation allowed the Effective Radiated Power (ERP) to be determined as well. Using the geolocations to infer the ERP, we further narrowed the data according to peak ERP for the 130-MHz-band: ERP >0.2 kW for the less stringent, and >2 kW for the more stringent data sets.

Extending the geolocation to all recorded discharges inferred to be in a given storm, using the borrowed geolocation from a subset of that storm's recorded discharges, results in a larger geolocated data set than would available with strict coincidence. However, this extension also includes many VHF recordings for which no coincident sferic or optical "ground truth" data were recorded.. Thus this article does not (and can not) address the detailed relationship of the VHF signal and other signals (either sferic or optical).

Table 1 summarizes the two selected data sets. We emphasize that cited thresholds are for the 130-MHz passband, not the 38-MHz passband which is more familiar in FORTE technical publications. Using the 130-MHz passband as the control band for data selection tends even further to exclude the narrow, coherent intracloud signals characteristic of progressing leaders. That is because the narrow, coherent signals have been shown to have a steeper spectral roll-off versus frequency in the VHF, and in the 130-MHz band their power is small compared to the power of the wide events (Jacobson et al., 1999).
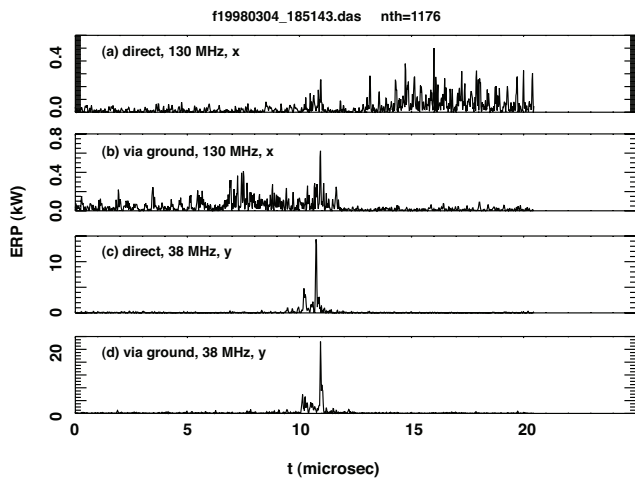
Fig. 2. Dechirped, prewhitened effective radiated power (ERP) versus t, for a typical low-energy, narrow intracloud VHF pulse. This pulse is typical of those not selected for the present study. **(a)** Direct path, 130 MHz, antenna x. **(b)** Via ground, 130 MHz, antenna x. **(c)** Direct path, 38 MHz, antenna y. **(d)** Via ground, 38 MHz, antenna y.

Fig. 3. Dechirped, prewhitened effective radiated power (ERP) versus t, for a typical high-energy, wide intracloud VHF pulse. This pulse is typical of those selected for the present study. **(a)** Direct path, 130 MHz, antenna x. **(b)** Via ground, 130 MHz, antenna x. **(c)** Direct path, 38 MHz, antenna y. **(d)** Via ground, 38 MHz, antenna y.

5   Examples of data records

We first illustrate how using the 130-MHz band as the control on data selection will help to exclude coherent intracloud leader pulses. Figure 2 shows time series of ERP from just such a discharge that we wish to exclude. (The ERP is calculated using the sum of the squares of the measured electric field and the Hilbert transform of the electric field. This gets rid of the uninteresting nulls due to the oscillatory nature of the measured E.) This event in Fig. 2 is excluded from the allowed data sets due to the criteria on contrast and SNR of the 130-MHz channel. The direct path, and the path via ground, are shown in their own separate panels, with appropriate time-shifting to align them. The direct-path ERP is shown for (a) 130 MHz and (c) 38 MHz, while the ERP from the path via ground is shown separately, for (b) 130 MHz and (d) 38 MHz. The 38-MHz ERP acts like a single coherent pulse, with better dechirping in this particular case for the slower-propagating, and more temporal spread for the faster-propagating birefringent modes. The 38-MHz ERP's wide pedestal is exclusively due to birefringence and residual dispersion. The 38-MHz ERP via the ground is a close replica of the 38 MHz ERP from the direct path. The peak 130-MHz ERP is weaker (by a factor of $\sim$25) and fails to show any distinct peak at all. This is typical of the leader-type intracloud discharges which have narrow, coherent signals at 38 MHz, but which degrade into extended, low-amplitude noise at 130 MHz, due to steep spectral rolloff. Figure 2, then, illustrates the kind of event that is not selected in this study.
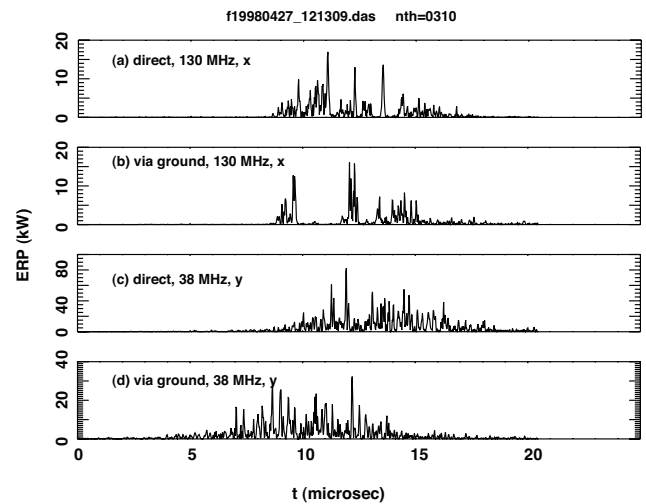
Next, we show in Fig. 3 a typical event that meets the criteria not only for the less stringent, but also for the more stringent data set (see Table 1). The format of Fig. 3 is unchanged from the previous figure, but the pulse behavior is dramatically different in four ways:

First: The envelope of power in both frequencies is wide-on the order of 10 µs.

Second: The ERP at 130 MHz is within a factor of $\sim$3 of the ERP at 38 MHz.

Third: The ERP envelope at 130 MHz appears to consist not only of random variations, but also of quasi-discrete distinct peaks. (This feature is always less distinct at 38 MHz, principally due to birefringent mode doubling and residual dispersion (Massey et al., 1998b; Roussel-Dupré et al., 2001).)

Fourth: Curiously, the detailed substructure of the 130-MHz ERP is quite different between the two views of the discharge. Apart from overall envelope duration ($\sim$10 µs), Fig. 3a, b shows essentially no detailed correlation between the two internal structures at 130 MHz. (The same cannot necessarily be said for 38 MHz, because the internal structure is too confused by birefringence and other residual dispersion (Massey et al., 1998b; Roussel-Dupré et al., 2001).) This dramatic difference of internal pulse structure between the two views at 130 MHz is troubling, given that all that is done differently in the measurement is use of different observing angles.

6 Potential antenna biases

The key departure of the results to follow is to take advantage of the dual geometrical views of the emission process afforded a satellite-based transient-recording payload. In the work to follow, we are primarily interested in the relationship between the signals in the two views. The first view is along the direct path from the intracloud discharge to the satellite. The second view is from the intracloud discharge to the specular ground and thence to the satellite (see Fig. 1a). We are justified (Massey et al., 1998a; Tierney et al., 2002) in assuming specular reflection at the surface. When the satellite is at zenith, the two views of the emission region are 180 deg opposed, and when the satellite is on the horizon, the two views are almost parallel. For most satellite positions (relative to the lightning) the two views are substantially oblique to each other, at an angle between those extremes.

A potential bias is introduced by the FORTE antennas, and the data analysis must seek to avoid effects of this bias. Consider the satellite-frame coordinates x, y, z. Here z is along the anti-nadir direction (outward into space from the Earth's center through the satellite), x is across the ram direction and to the right side of the orbit, and y is along the ram direction. The antenna consists of two orthogonal log-periodic antennas, one (the "x antenna") whose E-plane is the xz plane, and the other (the "y antenna") whose E-plane is the yz plane. The antenna in Figs. 2 and 3 is labeled as "x" or "y".

From FORTE's 800-km orbital altitude, the Earth's visible disk is approximately 3000 km in radius. The limb of the Earth is near 63 deg nadir angle, seen from the satellite. The antenna response is designed to be almost flat in the H-plane over this disk, and to smoothly taper (from a peak at nadir) in the E-plane. The 38-MHz E-plane taper of each antenna has been studied by extensive fitting of geolocated data (Jacobson and Shao, 2002a; Shao and Jacobson, 2001), and is determined to behave as follows, at least in the range up to 63-deg nadir:

$$G = \text{sinc}^2(w\alpha) \qquad (1)$$

Here, G is the antenna's power gain relative to nadir, α is the projection of the source vector angle onto the antenna's E-plane, in radians, and w is a rate-of-variation versus angle, fitted to ∼1.8 for the 38-MHz band, corresponding to a first null beyond the Earth's limb. This is a very broad response, allowing all regions of the disk to be seen even in the E-plane (albeit with a rolloff), and with almost no rolloff in the H-plane. For 130 MHz, the H-plane response is similarly broad, while the E-plane response varies (with w increasing proportionally to frequency) more rapidly versus α than it does at 38 MHz. That creates a single-sidelobe structure, placing a single null within the Earth's disk's intersection with the E-plane, with a rate of variation of gain versus α scaling to $w \sim 5$ in Eq. (1).

The two views of the discharge (direct path, and path via ground) arrive at the satellite at different angles. If the source
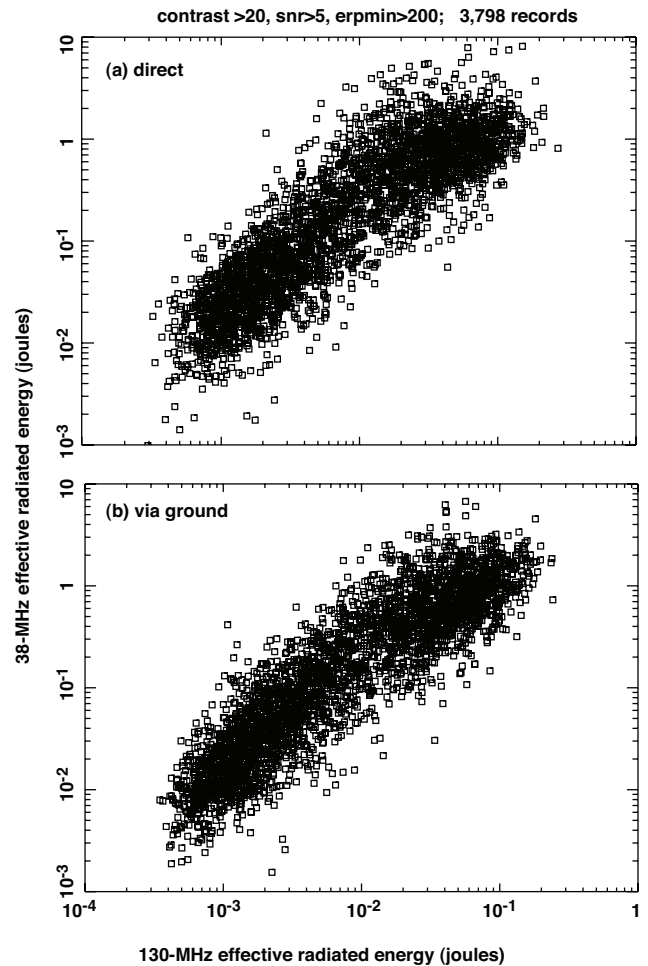

Fig. 4. Scatter plot of effective radiated energy (J), using the less-stringent event set. Each point shows 38-MHz (vertical axis) vs. 130-MHz (horizontal axis) energy of a pulse. **(a)** Direct path. **(b)** Path via ground.

lies in the H-plane, this makes no difference. If the source lies in the E-plane, the difference is maximized. In the process of solving for the intracloud-emission height we also solve for the angle-of-incidence onto the satellite (Jacobson et al., 1999), and it is straightforward knowing the geolocation and satellite ephemeris to project that vector incidence onto both the E- and H-planes (Jacobson and Shao, 2002a). Doing this, we find that α seldom differs between the direct path and the path via ground by more than ∼0.03 rad, so that the difference in 130-MHz antenna sensitivity (see Eq. 1) between the two paths should be negligible for most lines-of-sight, provided the measurements of the first and second peaks (in the TIPP) are always done on the same antenna. This is assured- the 400-µs recorded waveform on a given antenna easily contains both the paths' contributions (see Fig. 1b, c).
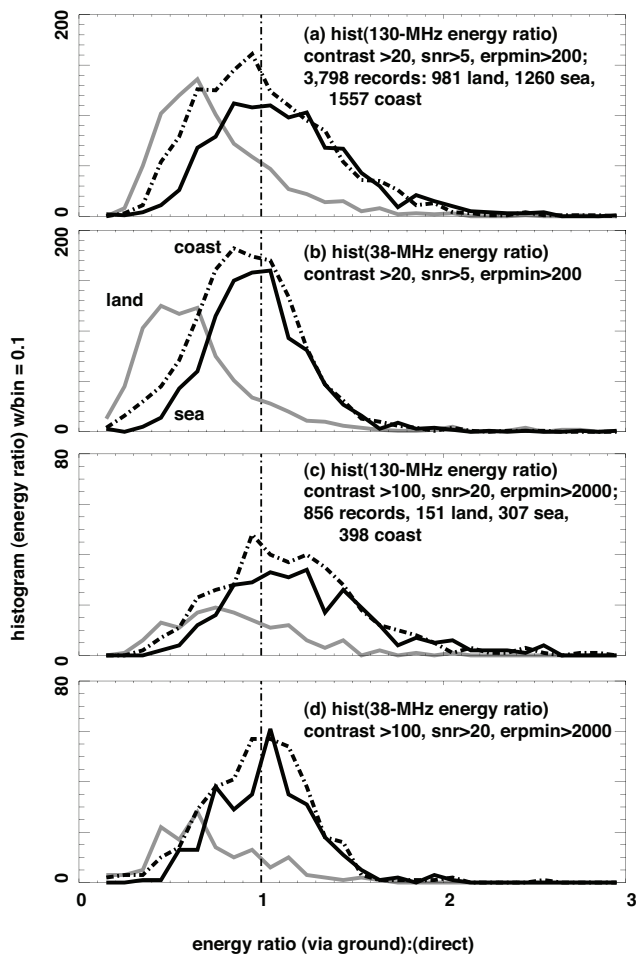
Fig. 5. Histograms of (via ground)/(direct) pulse-energy ratio. Lightning locations separated according to being on sea (dark solid curve), coastal (dark dashed curve), and land (grey solid curve) areas. Vertical dashed line indicates unity energy ratio. **(a)** 130-MHz energy ratio, for less-stringent event set. **(b)** 38-MHz energy ratio, for less-stringent event set. **(c)** 30-MHz energy ratio, for more-stringent event set. **(d)** 38-MHz energy ratio, for more-stringent event set.

7 Statistical results

7.1 Total emitted energy at 38 MHz and 130 MHz

The time-integrated ERP during a pulse's entire duration gives the effective radiated energy. Figure 4 is a scatter plot of 38-MHz (vertical scale) versus 130-MHz (horizontal scale) effective radiated energy for the less-stringent data set (Table 1), ignoring antenna effects. The scatter plots are separately shown for (a) the direct path, and (b) the path via ground. Much of the scatter is attributable to ignoring antenna effects, but the point of this figure is to demonstrate that statistically the variance of 38-MHz energy mimics the variance of 130-MHz energy, albeit with $\sim$ tenfold more energy at 38 MHz than at 130 MHz.

Table 2. Fraction of recordings with energy ratio (via ground)/(direct) >1.

Surface/frequency band	Contrast >20, snr >5, ERP >0.2 kW	Contrast >100, snr >20, ERP >2 kW
Land/130 MHz	0.14	0.24
Coast/130 MHz	0.40	0.59*
Sea/130 MHz	0.54*	0.65*
Land/38 MHz	0.09	0.14
Coast/38 MHz	0.33	0.41
Sea/38 MHz	0.34	0.45

7.2 Ratio of total energy (path via ground)/(direct path)

Using exclusively the wide-pulsetrain data sets (Table 1), we now repeat the approach of T2002 and calculate, in each recording, the ratio of energy along the path via ground, to the energy along the direct path. Figure 5a shows histograms of the 130-MHz energy ratio for lightning locations over land (grey solid curve), ocean (black solid curve), and coastal areas (black dashed curve), for the less-stringent data set. Figure 5b shows the accompanying 38-MHz ratio histograms. Then the exact same exercise is shown for the more stringent data set in Fig. 5c, d. What is striking is that the energy ratio for the 130-MHz band tends to be distributed to a higher range than is the energy ratio for the 38-MHz band, in any subset (less/more stringent, and land/coast/sea).

Table 2 summarizes the fraction of recordings for each case that have energy ratio >1. For the less stringent data set, 54 % of the 130-MHz ratios over sea are >1, while for the more stringent data set, 65 % of the 130-MHz ratios over sea are >1. The 38-MHz ratios are consistent with those reported by T2002, which used only that lower-frequency band.

T2002 identified two reasons why it is possible to have ratios >1 for the 38-MHz data they used: First, the "antenna lobe" of polarized emitters could have different gain along the two views. This has been explicitly demonstrated elsewhere (Jacobson and Shao, 2002a) with examples of coherent leader pulses. Second, the antenna lobe of the FORTE antenna could introduce a bias against the lower-elevation-angle (direct) propagation path. These two effects both involve antenna lobes, the first effect being the antenna lobe of the emitter, and the second effect being the antenna lobe of the receiver.

This study, by incorporating the 130-MHz band, extends the findings of T2002. Not only are there many events individually having more power on the path via ground than on the direct path, but for the 130-MHz band more than 50 % of the events are in this category. This is sufficiently troubling that we must ensure against instrumental biases from the FORTE antenna. Fortunately the use of geolocated lightning discharges allows us to reconstruct the precise geometry of

the event's two propagation paths in satellite coordinates (Jacobson and Shao, 2002a). Thus we can retrieve the angle α (see Eq. 1) individually for each event, taking into account the position of the lightning, the orientation and position of the satellite, the ram direction, and the assignment of which of the two possible antennas (x, or y) is used for that recording. We do this for all 130-MHz records in each data set (Table 1), and then stratify the data into two equally-populated halves of the angle α in the E-plane. From the discussion in Sect. 6 above, we would anticipate that the effect of antenna-lobe bias, if detectable, would manifest itself as a systematic difference between the event-set's subset with small angle α versus the subset with large angle α. The response lobe of the FORTE antenna is controlled by the angle α in the E-plane (Eq. 1), rather than by the nadir angle, because the H-plane response is almost uniform (Jacobson and Shao, 2002a). We take all the sea + coastal data in each data set and (not shown) repeat the histograms of the energy ratio for two halves of the E-plane-angle (α in Eq. 1) distribution. We find that there is no significant difference between the two halves of the sea+coastal result when it is stratified in that manner. Therefore we conclude that the higher-than-expected energy ratios for 130 MHz in Fig. 5 are not an artifact of the slightly different E-plane angles of the direct path and the path via ground.

We conclude from Fig. 5 that, troublingly, the distribution of 130-MHz power on the path via ground is anomalously strong compared to what can be reasonably expected for a reflected replica of the direct-path power. (This cannot be said of the 38-MHz data.) This is the second troubling finding, the first having been the observed lack of detailed correspondence between the features in the 130-MHz ERP on the two views of the same discharge.

Another reinforcement of this troubling result is seen in the co-variance of the 38-MHz and the 130-MHz energy ratios, which is shown as a scatter plot in Fig. 6 for the less-stringent data set. The straight grey line is the equality line. Clearly at the higher ratio values, i.e., energy ratio >1.3 on the abscissa, the trend of increase favors the 130-MHz ratio more than the 38-MHz ratio. This is consistent with the higher energy ratios for 130 MHz than for 38 MHz in the histograms of Fig. 5a, b.

In order to gain further insight on this phenomenon, we again pool-together the data for both coastal and sea lightning locations to get strong statistics, and plot in Fig. 7 the effective radiated energy on the path via ground (vertical axis), versus the effective radiated energy on the direct path (horizontal axis). The less stringent data set is treated in the top row, while the more stringent data set is in the bottom row. The left column contains the 130-MHz data, and the right column the 38-MHz data. The equality line is also shown in each panel. It is apparent that for 130-MHz radiated energy >0.05 J on the direct path, the 130-MHz energy on the path via ground more often is above the equality line than below (Fig. 7a, c).
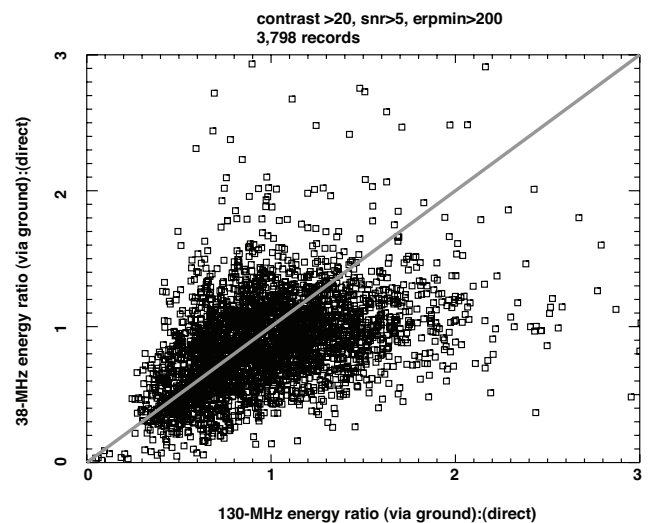

Fig. 6. Scatter plot of 38-MHz (vertical axis) vs 130-MHz (horizontal axis) pulse-energy ratio (via ground)/(direct), using the less-stringent event set.

7.3 ERP time-variations within the pulse envelope

We need to define the pulse-envelope start and stop times, so that the data can be analyzed automatically for characteristics of the internal structure of the pulse. We choose to use an energy-based definition: the pulse boundaries will be taken as the time window containing the inner 80 % of the energy of the pulse, thus the period between the times of passage through the 10 % and 90 % levels in time-integrated ERP. This is separately determined for each propagation path (direct, and via ground). We now have a uniform definition of the temporal extent of each pulse.

Using the 10 %/90 % boundaries, we show in Fig. 8 the distributions of instantaneous ERP for (a, c) 130 MHz and (b, d) 38 MHz. The top row (a, b) is for the less-stringent event set, while the bottom row (c, d) is for the more-stringent set. In each panel the solid curve is the distribution for the direct path, while the dashed curve is the distribution for the path via ground. Both the abscissa and the histogram's bin are logarithmic. A data point is accumulated every sample interval (0.02 μs) during each pulse studied, since this distribution is for the instantaneous ERP. The data is limited to the good-reflector conditions, namely sea + coast, excluding land. It is apparent that the instantaneous 130-MHz ERP on the path via ground is distributed slightly higher than is the ERP on the direct path (see Fig. 8a, c), especially in the more-stringent data set (Fig. 8c). The difference is less apparent, and possibly of opposite sign, for 38-MHz data (Fig. 8b, d).

We now quantify the degree of temporal similarity between the ERP time series for the two paths. Figure 9 shows the time-lagged autocorrelation (solid curve) of 130-MHz ERP for the less-stringent data set, for (a) the direct path and
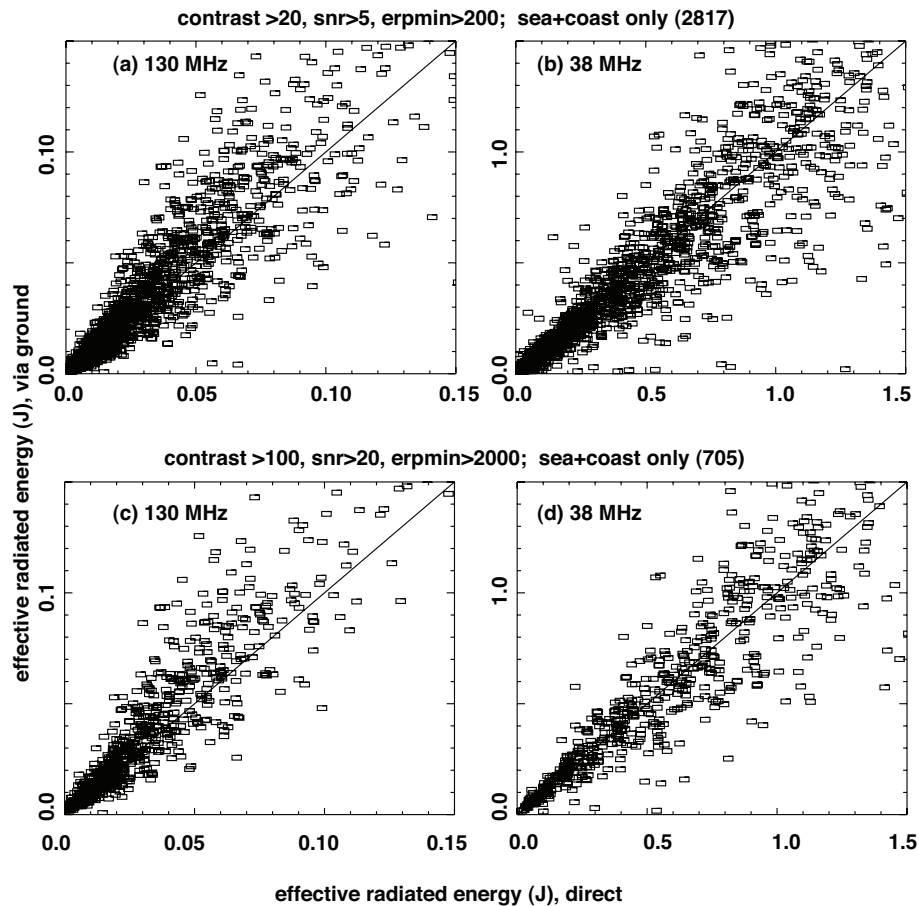
Fig. 7. Scatter plots of effective radiated energy for path via ground (vertical axis) vs. direct path (horizontal axis). Panels on left (**a**, **c**) are for 130 MHz, while panels on right (**b**, **d**) are for 38 MHz. Top two panels (**a**, **b**) are for all 2817 sea + coastal pulses within the less-stringent event set, while the bottom two panels are for all 705 sea + coastal pulses within the more-stringent event set.

(b) the path via ground. The two autocorrelations are quite similar, showing a sharp, large-scale decorrelation in 0.2 µs or less (slightly longer for the path via ground than for the direct path). The ERP is a non-negative variable with a finite mean within the pulse, so the fast decorrelation transitions to a slower decorrelation outside of ±0.2 µs. The dashed curve shows the lagged cross correlation of the ERP in the path via ground, relative to the direct path. The cross-correlation requires care to avoid trivial results: To prepare this statistic, one must first align the two envelope onsets of the two paths. After performing this alignment and accumulating the cross-correlation, we see that most of the short-term correlation is entirely missing in the cross-correlation, which recapitulates only the slower pedestal of the autocorrelations. In other words, the rapidly-varying features (variations on timescales <0.2 µs) of the ERP are essentially uncorrelated between the two paths. This shows statistically what was visually obvious for the one case example of Fig. 3a, b. It is a basic difference between the wide-pulse discharges studied here, on the one hand, and, on the other hand, the low-band

narrow, coherent events (Fig. 2c, d). In those events, the 38-MHz narrow feature in the path via ground is a clear replica of the 38-MHz narrow feature in the direct path.

As was noted with Fig. 3a, b, the 130-MHz ERP contains irregularly spaced narrow peaks. We will now examine two common statistical measures (Rusbridge and Jacobson, 1984) of the importance of such peaks within the overall ERP distribution. Each of these statistics tests the degree to which the energy is concentrated into unusually large, quasi-discrete peaks or "spikes". The first statistic is the ratio of the maximum ("peak") ERP amplitude to the median of the ERP for a given event and path, within a given event's 10 %/90 % pulsewidth. The second is the kurtosis, which is the mean fourth-power of the electric-field envelope over the square of the mean second power of the electric-field envelope. The ERP is already proportional to the second power of the envelope of E. Thus the kurtosis of the envelope is the mean square of the ERP divided by the square of the mean ERP, within a given event's 10 %/90 % pulsewidth. For both of these statistics, each event gives one datum per event/path.
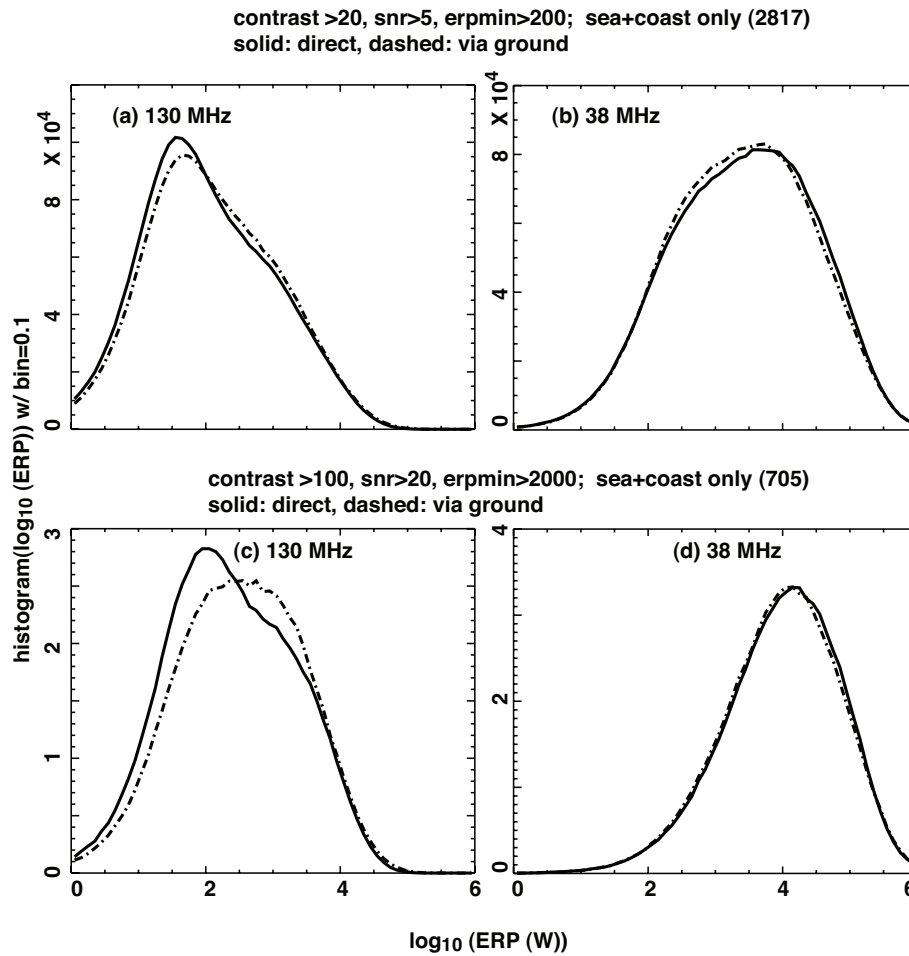
Fig. 8. Histograms of instantaneous log10 (ERP) for **(a)**, **(c)** 130 MHz on left and for **(b)**, **(d)** 38 MHz on right. Top two panels **(a, b)** are for all 2817 sea + coastal pulses within the less-stringent event set, while the bottom two panels **(c, d)** are for all 705 sea + coastal pulses within the more-stringent event set. Solid curve: direct path; dashed curve: path via ground. An ERP statistic is accumulated each 0.02 μs within the 10 %-to-90 % pulse duration of each event.

Figure 10 shows (a, c) histograms of the peak ERP divided by the median ERP, and (b, d) histograms of the kurtosis. The upper row (a, b) is for the less-stringent data set, while the lower row (c, d) is for the more stringent data set. In each panel the solid curve is for the direct path, while the dashed curve is for the path via ground. Figure 10 indicates that both the peak ERP divided by the median ERP, and the kurtosis, are distributed higher for the signal arriving via ground than for the signal arriving via the ground path. This implies that the signal arriving via ground is more dominated by quasi-discrete peaks.

Another statistic indicating the importance of quasi-discrete peaks is the distribution of instantaneous ERP divided by the event's mean ERP. This accumulates an additional datum each 0.02 μs within the 10 %/90 % pulsewidth, in contrast to Fig. 10 which gathered only one datum for each event. Figure 11 shows this distribution for (a) the less stringent and (b) the more stringent data sets. The solid curve is

for the direct path, while the dashed curve is for the path via ground. Note the logarithmic ordinate scale. Also shown is a thin straight line indicating a Rayleigh distribution of the electric-field envelope, in which ERP/<ERP> would be expected to be an exponential (Beckman, 1964). The Rayleigh distribution would be expected if the signal were caused by random fading due to a summation of numerous uncorrelated inputs. An example of this situation would be the signal from corona breakdown with numerous breakdown loci all contributing to the received signal. Clearly, the overall ERP/<ERP> distribution shows a clear departure from random fading. The upwards-positive curvature of the histograms is due to the concentration of energy into discrete high peaks, compensated by more "zeroes" or near-zeroes in the ERP. This behavior is dramatically illustrated by the example time series in Fig. 3a, b.

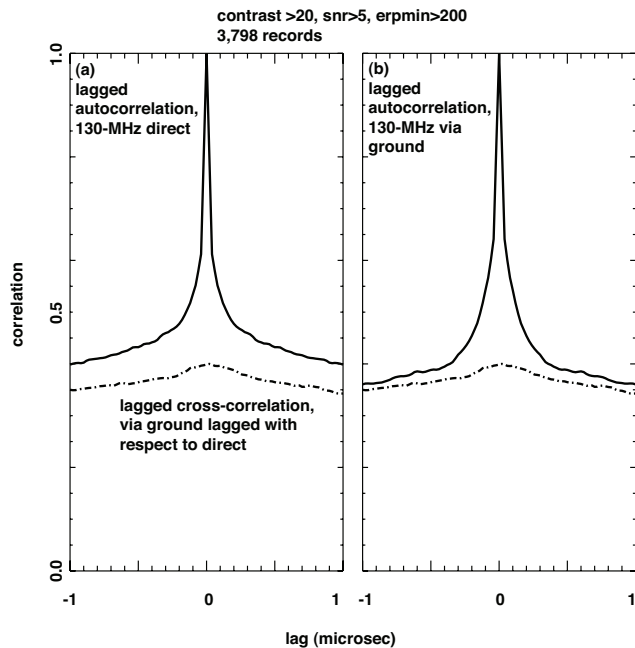The tendency in Fig. 11 for the path via ground to have more counts than the direct path is due to the difference in

Fig. 9. Lagged autocorrelation (solid curve) of instantaneous 130-MHz ERP, for **(a)** direct path and **(b)** path via ground, using all events in the less-stringent event. Dashed curve is the lagged cross-correlation of the path via ground with respect to the direct path, after syncronizing the pulse start of the two paths for each event record.

the distribution of pulse-width. To quantify this, Fig. 12 shows scatter plots of the 130-MHz, 10 %/90 % pulsewidth, for (a) the less stringent and (b) the more stringent data sets. In each panel the equality line is shown in grey. The pulse-width for the path via ground tends, on average, to exceed the pulsewidth for the direct path, by about 1–2 μs. This is true in either data set.

8 Quasi-repetitive bursts

Figure 3a presented a direct-path, 130-MHz ERP time history that appears to show recurrence of four pulses at a quasi-regular interval (∼1.5 μs). However, the pattern is not at all reproduced in the path via ground. Moreover, given that we have examined by eye literally hundreds of time records, and given how biased human perception is for regular patterns, we are cautious about this and other apparent recurrences.

A similar apparent recurrence is seen in Fig. 13, showing the 130-MHz ERP (from a different recording than Fig. 3), for (a) direct path and (b) path via ground. In this example, the apparent recurrency is seen in the path via ground, in the time range $t = 3$ to $t = 6$ μs. The apparent period of recurrence is ∼0.5 μs, but that period is not steady. Moreover, this recurrent pattern is brief even where it occurs, and is absent in the direct path.

When the discrete peaks are visible, which is in only a portion of the records, the apparent recurrence period varies from record to record, and is unsteady in even one record. The string of apparent recurrency rarely occupies most of the pulse width. Finally, the recurrency does not correlate between the direct path and the path via ground.

As noted earlier, the VHF emissions originally reported by Le Vine were associated with simultaneous sferics, thus with major current flows (Le Vine, 1980). A later study inferred that many, perhaps most, of the strong intracloud VHF emissions were not accompanied by a large-scale current (Jacobson, 2003b), so this matter is perhaps not yet certain. Recently, finer-scale oscillations in the NBP sferic have been reported (Nag and Rakov, 2009, 2010a, b; Nag et al., 2010) and interpreted as a bouncing-current effect of the NBP channel acting like an imperfectly-terminated transmission line.

Given our observations of quasi-periodic VHF recurrent peaks within the VHF waveform, the question arises, are the VHF peaks an aspect of the same phenomenon as the reported sferic oscillations? Our data are incapable of addressing that.

First, there is only rarely a recorded coincident LASA sferic waveform ground-truthing our FORTE data. LASA did not begin to ground-truth FORTE systematically until 1999, by which time FORTE's dual-frequency VHF recordings had been replaced by single-frequency (38-MHz) recordings. Second, the LASA sampling during the FORTE recordings was at 1 sample/microsec, with an analog 300-kHz low-pass filter, for a Nyquist period of ∼3 μs. On the other hand, the finer-scale sferic oscillations reported by Nag et al. have periods on the order of 1 μs (see Fig. 2b in Nag and Rakov, 2010a) and display a remarkably "high-Q" oscillatory quality factor. The LASA-concident sferic-waveform data, during the FORTE VHF recordings, would have lacked the bandwidth to resolve the sferic oscillations reported by Nag et al. In addition to this technical difficulty, we note that the recurrences we see in the VHF are at best quasi-periodic, and these apparent recurrences of VHF peaks seldom extend more than a few repetitions. The oscillations reported by Nag et al., on the other hand, extend several sinusoidal periods at a sensibly constant period (see, e.g., Fig. 1 in Nag and Rakov, 2009).

Notwithstanding the low probability that LASA with its bandwidth limit could even observe the bouncing-wave phenomenon, we have combed through an extensive and well-documented LASA sferic-waveform NBP data set (Jacobson et al., 2007) but have found no multi-period oscillations suggestive of the bouncing-wave signature. We note however that a single secondary peak has been reported in some LASA waveforms of NBPs (Hamlin et al., 2007), without ringing oscillations, but it is not evident that this secondary peak and the phenomena reported by Nag et al are the same process. Thus, we can not at this time even infer whether our observed VHF-peak recurrences are related to the sferic
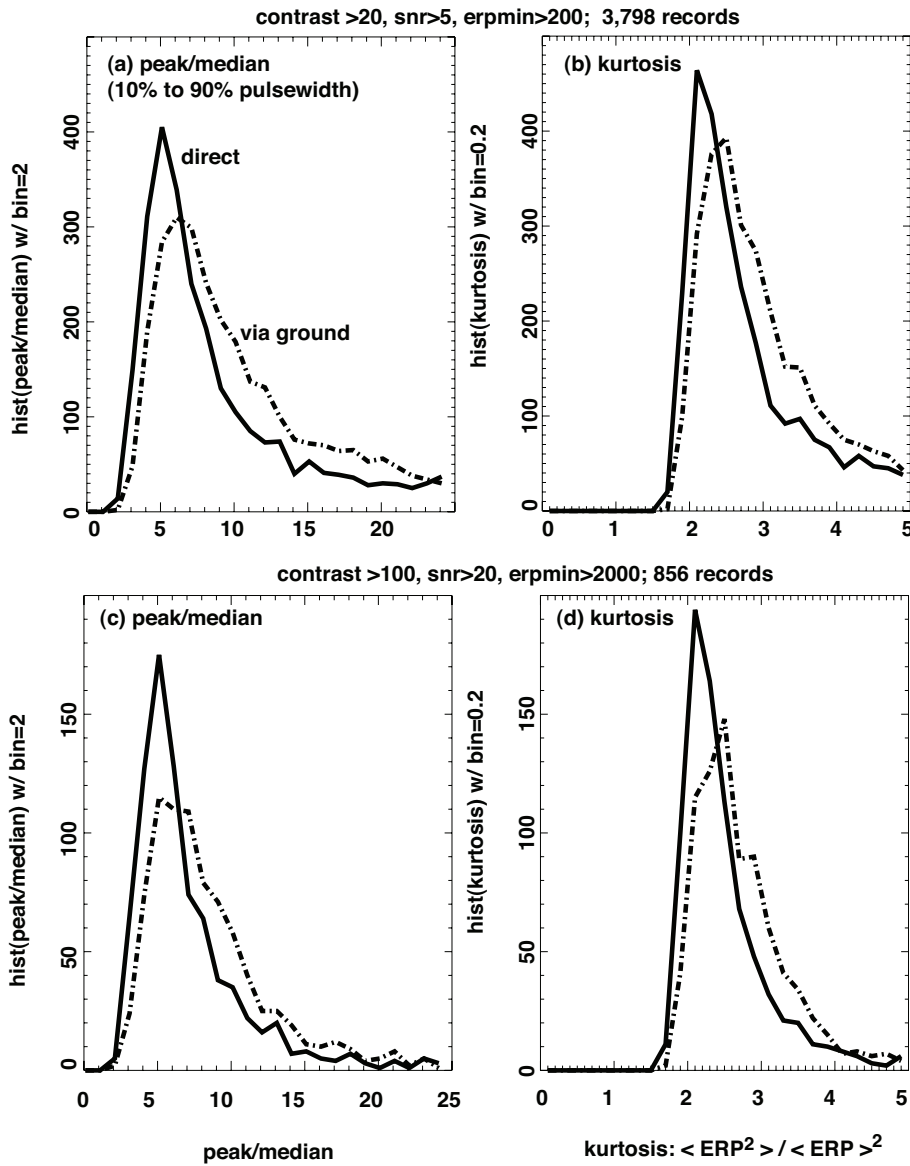
Fig. 10. Histograms of **(a)**, **(c)** the ratio of peak/median ERP, and **(b)**, **(d)** the kurtosis of electric-field envelope, for 130-MHz pulses. Top row **(a, b)** is for the less-stringent event set, while bottom row **(c, d)** is for the more-stringent event set. Solid curve: Direct path; dashed curve: path via ground. The two characteristics of each event are determined by the 10 %-to-90 % duration of that event.

oscillations reported by Nag et al. We feel that the limited LASA bandwidth prevented addressing this question.

9 Implications of a spatially-extensive VHF source

The VHF emissions for the recordings selected in this study may originate in sources of finite spatial extent. At least five studies have sought to infer, among other parameters, the physical length of the intracloud emission region associated with NBPs. The original estimate (Smith et al., 1999) was of a length in the range of 0.3–1 km, inferred from trade-offs of the measured charge-moment change of the sferic, dura-

tion of HF emission accompanying the sferic, and a range of reasonable propagation velocities for a front traversing the length of the channel. This inference could not be made a certainty, but used a reasonable trade-off of parameters (length, front velocity, charge transfer, etc.) to avoid non-physical conditions. The second estimate of the length of the emission region (Eack, 2004) did not need to include the HF/VHF noise duration, but instead used sferic recordings in which the lightning was sufficiently close that the sferic's electrostatic and inductive signals were recorded on that one station, in addition to the usual radiated component seen at more distant stations. This allowed an estimate of the length
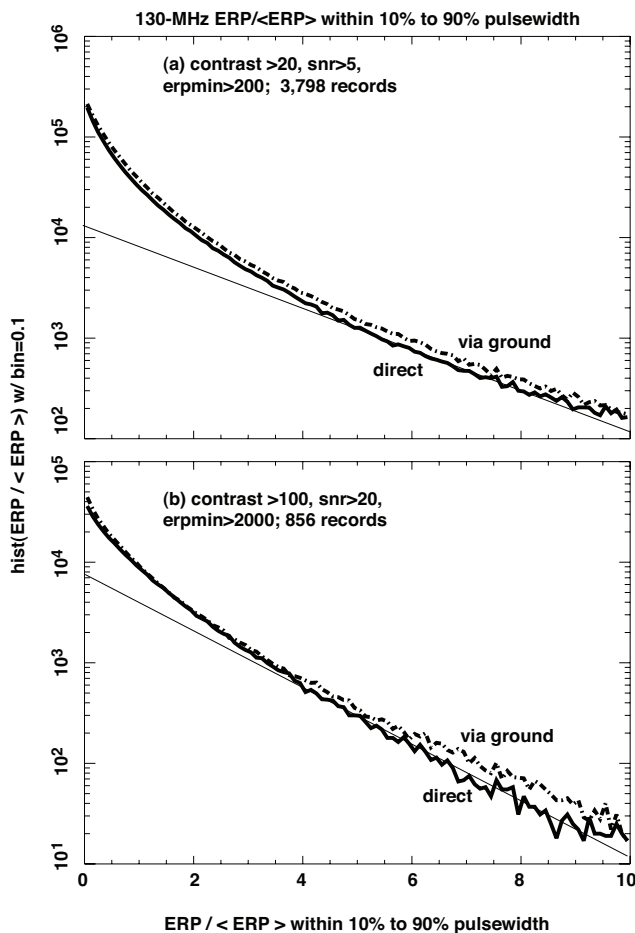
Fig. 11. Histogram of the ratio of instantaneous ERP to pulse-averaged <ERP>, for **(a)** the less-stringent event set, and **(b)** the more-stringent event set. Heavy solid curve: direct path; heavy dashed curve: path via ground. Light solid tangent line: Rayleigh-fading behavior. Note the logarithmic vertical scale. An ERP-ratio statistic is accumulated each 0.02 µs within the 10 %-to-90 % pulse duration. The average <ERP> in the ratio's denominator is computed for each pulse individually.

Fig. 12. Scatter plots of 10 %-to-90 % pulse width at 130 MHz, for path via ground (vertical axis) vs. direct path (horizontal axis). Grey line is for equality of the two. **(a)** Less-stringent event set. **(b)** More-stringent event set.

as averaging ∼3 km, notably longer than the original inference. (However, this estimate has recently been questioned by other authors (Nag and Rakov, 2010b).) The third study to estimate a discharge length (Hamlin et al., 2007) based its inference on a secondary peak (on the decaying flank of the sferic) interpreted as a current-wave reflection from an unterminated channel. The inferred length was ∼2 km, between the estimates from previous studies. The fourth study providing a length estimate was a comparison of Transmission-Line and Modified-Transmission-Line models (Watson and Marshall, 2007). These authors (see their Table 2) inferred a NBP channel length of ∼600 m if they assumed a velocity of $6 \times 10^7 \, \mathrm{m \, s^{-1}}$. The fifth study to attempt a discharge-length estimate (Nag and Rakov, 2009, 2010a, b; Nag et al., 2010) inferred lengths in the range 0.1 to 0.15 km, based on the bouncing-wave idea.
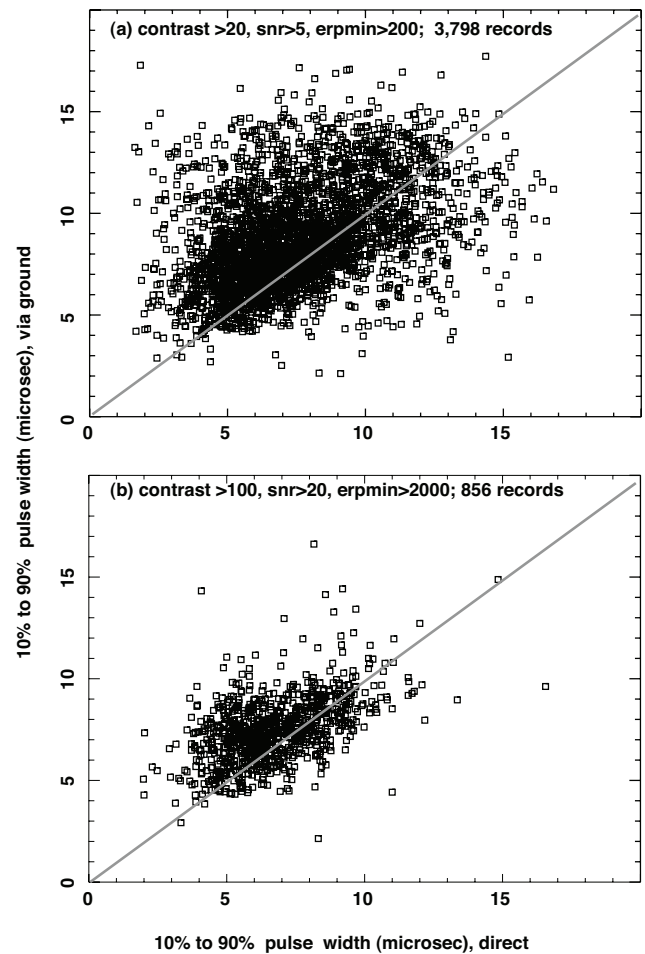
Since the physical models underlying these five length estimates are different, it is perhaps not surprising that the results differ. Each model involves some speculation. Another possibility is that one or more of the underlying models are not relevant to the recorded data. At any rate, there is an interesting implication of nonzero spatial extent for the current study of multi-microsecond VHF emissions from intracloud discharges.

This study has demonstrated the troubling feature that time-dependent details of the 130-MHz internal pulse structure are essentially uncorrelated between the direct path and the path via ground. In part, this might (in principle) be explainable by finite source dimension. Consider a simplified cartoon in Fig. 14, in which we model the simplest case of a spatially-diverse emission region: The VHF emission region is assumed to comprise only two spatially separated emitters, and this is further simplified into one dimension, by assuming that the two emitters are only vertically separated, and
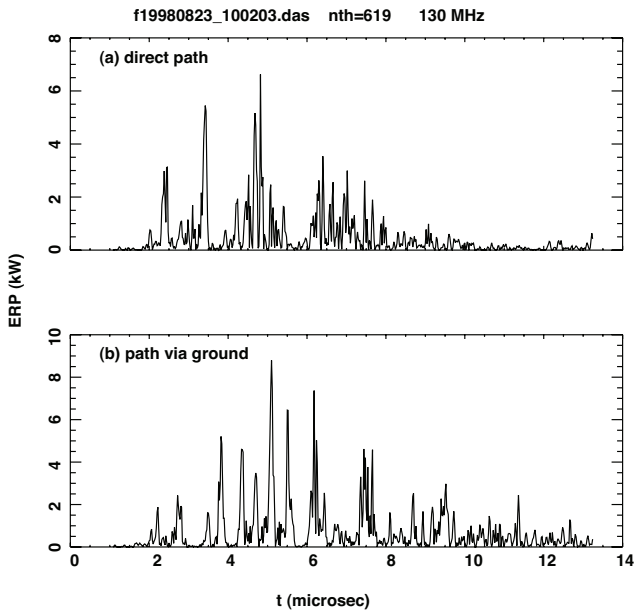
Fig. 13. 130-MHz ERP vs. time for event nth=619 within file f19980823_100203.das. **(a)** Direct path. **(b)** Path via ground. The signals have been aligned to syncronize their leading rise as best as possible, and only 14 μs are shown for each propagation path.

Fig. 14. Simple one-dimensional case of a spatially-separated pair of discharge elements, at heights H_1 and H_2, along the satellite nadir axis.

that the satellite is at zenith. Let the satellite altitude be H_{sat}, the lower emitter's altitude be H_1, and the higher emitter's altitude be H_2. Suppose the two emissions occur punctually at times t_1, t_2 ($= t_1 + \tau$) respectively, where τ is the proper time difference of emission #2 with respect to emission #1. Then the two emitters' differential time-of-arrival (signal #2 minus signal #1 arrival times) at the satellite, along the "direct path", will be

$$W_{\text{dir}} = \tau + (H_1 - H_2)/c \qquad (2)$$

while the differential time-of-arrival at the satellite, along the "path via ground", will be

$$W_{\text{gnd}} = \tau - (H_1 - H_2)/c \qquad (3)$$

The differential time-of-arrival is the perceived "repetition interval" at the satellite. Comparing Eq. (2) with Eq. (3), we see that the two views of the same two-emitter process from the satellite will furnish different estimates of the "repetition interval", W. Pursuing this further, suppose the proper time difference τ is due to progression of a front at a speed v. If v is directed upward, then the pulse separation on the direct path will be reduced. On the other hand, if v is directed downward, then the pulse separation on the path via ground will be reduced. For the limit that v approaches c, then the two pulses can appear to merge.

The naive cartoon in Fig. 14 is not intended to be a "model" of our data, but only to speculate that the time relationship of emission peaks seen in the two views from the satellite can be significantly decorrelated simply by the finite
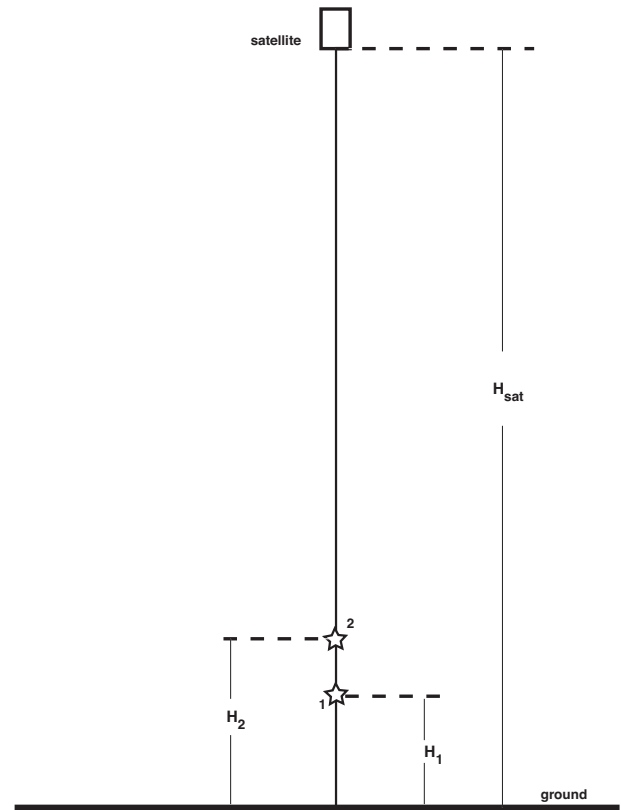
source dimensions. Complications include that the satellite elevation angle varies from 90 deg (the case shown in the cartoon) down to the horizon (0 deg) in our data sets, while the axis of the discharge (if there *is* an axis) can in principle be along any direction. Regarding the latter caveat, a recent Lightning Mapper Array study of blue jets and "bolt-from-the-blue" lightning shows how three-dimensional a thunderstorm can appear, and how this affects the lightning process (see, e.g., the radar-reflectivity image in Fig. 3a of Krehbiel et al., 2008). Thunderstorm charge separation needn't always occur between elegant horizontally-extensive strata in which the electric field is automatically vertical. Rather, small updraft cells can create surprisingly three-dimensional electric field configurations, and this local effect is further complicated by shielding charges accumulated at the cloud/clear-air boundary. Unlike the massive charge transfers (many tens of C) involved in those cloud-to-ground discharges associated with sprites (Rodger, 1999), the NBP intracloud discharge has been inferred to move very little charge, only a few tenths of a coulomb (Eack, 2004; Nag and Rakov, 2010b). Thus NBPs might arise in small-footprint and localized (and thus, non-planar) regions of electrical stress, while clearly the sprite-producing storms need to be able to collect charge coherently from a larger footprint, implying more planarity.

10 Speculation on effect of a relativistic "headlight" effect

High-speed optical measurements (e.g., Willett et al., 2008) show that cloud-to-ground return strokes develop via a progressing front, with relativistic speeds actually measured near or even exceeding $2 \times 10^8 \, \mathrm{m \, s^{-1}}$. With this insight, the far-field electric field measured at a sferic receiver e.g., in NLDN (Cummins et al., 1998; Cummins and Murphy, 2009), can be converted via the "transmission line model" (the theory for which is laid out in Uman et al., 1975) to a vertical-current estimate. By contrast, for intracloud NBPs, there is no access for optical time-resolved measurements of channel-front progression, and it is not known whether a front concept even applies in this setting. However, we note that the attempts to provide a conceptual picture of NBPs which were discussed with respect to inferring the length also attempt to infer the front speed (Eack, 2004; Hamlin et al., 2007; Nag and Rakov, 2010b; Smith et al., 1999). All of these estimates require a front speed near or exceeding $2 \times 10^8 \, \mathrm{m \, s^{-1}}$.

We neither endorse nor dispute the above estimates of front speed in NBPs. However, we mention an implication that such high-speed fronts would pose for the VHF radiation. It has already been shown with VHF radiation from negative cloud-to-ground strokes that the emission lobe is forward-beamed (relative to a dipole) (Shao et al., 2004, 2005), as appropriate for relativistic "headlight" effect. In that case the best-fit front velocity to account for the empirical beam lobe was $2.25 \times 10^8 \, \mathrm{m \, s^{-1}}$. We would therefore expect that, for the VHF pulsetrains studied here, a similar "headlight effect" would increase the potential differences between radiation into the "forward" and "backward" hemispheres.

11 Conclusions

This study has examined FORTE data on additional properties of the two VHF pulsetrains ("TIPPs") seen in a satellite recording for an energetic, multi-microsecond-duration intracloud discharge. Our findings include:

1. The FORTE high-band (130 MHz) reveals that each pulsetrain contains numerous quasi-discrete, narrow peaks. At 130 MHz, we can be sure that this oberved property is not an artifact of residual ionospheric dispersion and mode doubling. (At 38 MHz, these effects tend to blur such peaks.)

2. The quasi-discrete, narrow peaks in the pulsetrains are essentially uncorrelated between the two views of the discharge (direct path, and path via ground). Thus, we have avoided calling the signal arriving from the ground the "reflected signal", because that implies that otherwise it is the same signal as arrives on the direct path.

It is true that there is a reflection at the ground, but we have no evidence that the "reflected" signal behaves like a replica of the direct signal.

3. The 130-MHz energy arriving via the ground shows a statistically significant tendency to exceed the energy arriving along the direct path. This is not the case at the low band, 38 MHz.

4. The quasi-discrete peaks in the pulsetrain cause the amplitude distribution to be leptokurtic; the signal arriving via ground is slightly more leptokurtic.

5. The pulsetrain arriving via the ground has 1–2 µs additional width (based on energy), relative to the pulsetrain arriving on the direct path.

6. One can speculate that two processes might create some of the troubling dissimilarity between the pulsetrains along the different paths: spatially extended emission region, and relativistic "headlighting".

The properties listed above show that the most intense VHF associated with intracloud discharges is unlikely to be radiation from a simple, single dipole radiator. This fact will increase the challenge of modeling the radiation's origin and of understanding its relationship to other intracloud-lightning phenomena.

References

Beckman, P.: Rayleigh distribution and its generalizations, J. Res. NBS, 64D, 927–932, 1964.

Cummins, K. L., Murphy, M. J., Bardo, E. A., Hiscox, W. L., Pyle, R., and Pifer, A. E.: Combined TOA/MDF technology upgrade of U. S. National Lightning Detection Network, J. Geophys. Res., 103, 9035–9044, 1998.

Cummins, K. L. and Murphy, M. J.: An overview of lightning location systems: History, techniques, and data uses, with an in-depth look at the U. S. NLDN, IEEE Trans. Electromagnetic Compatibility, 51, 499–518, 2009.

Eack, K. B.: Electrical characteristics of narrow bipolar events, Geophys. Res. Lett., 31, L20102, doi:20110.21029/22004GL021117, 2004.

Hamlin, T., Light, T. E., Shao, X. M., Eack, K. B., and Harlin, J. D.: Estimating lightning channel characteristics of positive narrow bipolar events using intrachannel current reflection signatures, J. Geophys. Res., 112, D14108, doi:14110.11029/12007JD008471, 2007.

Holden, D. N., Munson, C. P., and Devenport, J. C.: Satellite observations of transionospheric pulse pairs, Geophys. Res. Lett., 22, 889–892, 1995.

Huang, Z. and Roussel-Dupré, R.: Total electron content (TEC) variability at Los Alamos, New Mexico: A comparative study: FORTE-derived TEC analysis, Radio Sci., 40, RS6007, doi:10.1029/2004RS003202, 2005.

Huang, Z. and Roussel-Dupré, R.: Total electron content (TEC) variability at Los Alamos, New Mexico: A comparative study: 2. Comparisons with other TEC sources, Radio Sci., 41, RS6004, doi:10.1029/2004RS003203, 2006.

Jacobson, A. R.: Relationship of intracloud-lightning radiofrequency power to lightning-storm height, as observed by the FORTE satellite, J. Geophys. Res., 108, 4204, doi:1029/2002JD002956, 2003a.

Jacobson, A. R.: How do the strongest radio pulses from thunderstorms relate to lightning flashes?, J. Geophys. Res., 108, 4778, doi:4710.1029/2003JD003936, 2003b.

Jacobson, A. R. and Light, T. E. L.: Bimodal radiofrequency pulse distribution of intracloud-lightning signals recorded by the FORTE satellite, J. Geophys. Res., 108, 4266, doi:4210.1029/2002JD002613, 2003.

Jacobson, A. R. and Shao, X.-M.: Using geomagnetic birefringence to locate sources of impulsive, terrestrial VHF signals detected by satellites on orbit, Radio Sci., 36, 671–680, 2001.

Jacobson, A. R. and Shao, X.-M.: On-orbit direction finding of lightning radio frequency emissions recorded by the FORTE satellite, 37, 4, doi:10.1029/2001RS002510, 2002a.

Jacobson, A. R. and Shao, X.-M.: FORTE satellite observations of very narrow radiofrequency pulses associated with the initiation of negative cloud-to-ground lightning strokes, J. Geophys. Res., 107, 4661, doi:4610.1029/2001JD001542, 2002b.

Jacobson, A. R., Knox, S. O., Franz, R., and Enemark, D. C.: FORTE observations of lightning radio-frequency signatures: Capabilities and basic results, Radio Sci., 34, 337–354, 1999.

Jacobson, A. R., Cummins, K. L., Carter, M., Klingner, P., Roussel-Dupré, D., and Knox, S. O.: FORTE radio-frequency observations of lightning strokes detected by the National Lightning Detection Network, J. Geophys. Res., 105, 15653–15662, 2000.

Jacobson, A. R., Holzworth, R., Lay, E., Heavner, M., and Smith, D. A.: Low-frequency ionospheric sounding with Narrow Bipolar Event lightning radio emissions: regular variabilities and solar-X-ray responses, Ann. Geophys., 25, 2175–2184, doi:10.5194/angeo-25-2175-2007, 2007.

Krehbiel, P. R., Riousset, J. A., Pasko, V. P., Thomas, R. J., Rison, W., Stanley, M. A., and Edens, H. E.: Upward electrical discharges from thunderstorms, Nature Geosci., 1, 233–237, 2008.

Le Vine, D. M.: Sources of the strongest rf radiation from lightning, J. Geophys. Res., 85, 4091–4095, 1980.

Light, T. E., Suszcynsky, D. M., and Jacobson, A. R.: Coincident Radio Frequency and Optical Emissions from Lightning, Observed with the FORTE Satellite, J. Geophys. Res., 106, 28223–28231, 2001.

Light, T. E. L. and Jacobson, A. R.: Characteristics of impulsive VHF lightning observed by the FORTE satellite, J. Geophys. Res., 107, 4756, doi:1029/2001/JD001585, 2002.

Massey, R. S. and Holden, D. N.: Phenomenology of transionospheric pulse pairs, Radio Sci., 30, 1645–1659, 1995.

Massey, R. S., Holden, D. N., and Shao, X.-M.: Phenomenology of trans-ionospheric pulse pairs: Further observations, Radio Sci., 33, 1755–1761, 1998a.

Massey, R. S., Knox, S. O., Franz, R. C., Holden, D. N., and Rhodes, C. T.: Measurements of transionospheric radio propagation parameters using the FORTE satellite, Radio Sci., 33, 1739–1753, 1998b.

Nag, A. and Rakov, V. A.: Electromagnetic pulses produced by bouncing-wave-type lightning discharges, IEEE Trans. Electromagnetic Compatibility, 51, 466–470, 2009.

Nag, A. and Rakov, V. A.: Compact intracloud lightning discharges: 1. Mechanism of electromagnetic radiation and modeling, J. Geophys. Res., 115, D20102, doi:20110.21029/22010JD014235, 2010a.

Nag, A. and Rakov, V. A.: Compact intracloud lightning discharges: 2. Estimation of electrical parameters, J. Geophys. Res., 115, D20103, doi:20110.21029/22010JD014237, 2010b.

Nag, A., Rakov, V. A., Tsalikis, D., and Cramer, J. A.: On phenomenology of compact intracloud lightning discharges, J. Geophys. Res., 115, D14115, doi:10.1029/2009JD012957, 2010.

Rodger, C. J.: Red sprites, upward lightning, and VLF perturbations, Rev. Geophys., 37, 317–336, 1999.

Roussel-Dupré, R. A. and Blanc, E.: HF echoes from ionization potentially produced by high-altitude discharges, J. Atmos. Solar-Terr. Phys., 60, 765–769, 1997.

Roussel-Dupré, R. and Gurevich, A. V.: On runaway breakdown and high altitude discharges, J. Geophys. Res., 101, 2297–2311, 1996.

Roussel-Dupre, R. A., Gurevich, A. V., Tunnell, T., and Milikh, G. M.: Kinetic theory of runaway air breakdown, Phys. Rev. E, 49, 2257–2271, 1994.

Roussel-Dupré, R. A., Jacobson, A. R., and Triplett, L. A.: Analysis of FORTE data to extract ionospheric parameters, Radio Sci., 36, 1615–1630, 2001.

Rusbridge, M. G. and Jacobson, A. R.: The analysis of fluctuating signals from a multi-chord interferometer, J. Appl. Phys., 56, 757–773, 1984.

Shao, X.-M. and Jacobson, A. R.: Polarization observations of broadband VHF signals by the FORTE satellite, Radio Sci., 36, 1573–1589, 2001.

Shao, X.-M., and Jacobson, A. R.: Polarization observations of lightning-produced VHF emissions by the FORTE satellite, J. Geophys. Res., 107, 4430, doi:10.1029/2001JD001018, 2002.

Shao, X.-M., Jacobson, A. R., and Fitzgerald, T. J.: Radio frequency radiation beam pattern of lightning return strokes: A revisit to theoretical analysis, J. Geophys. Res., 109, D19108, doi:10.1029/2004JD004612, 2004.

Shao, X.-M., Jacobson, A. R., and Fitzgerald, T. J.: Radio frequency radiation beam pattern of lightning return strokes: Inferred from FORTE satellite observations, J. Geophys. Res., 110, D24102, doi:10.1029/2005JD006010, 2005.

Smith, D. A., Shao, X. M., Holden, D. N., Rhodes, C. T., Brook, M., Krehbiel, P. R., Stanley, M., Rison, W., and Thomas, R. J.: A distinct class of isolated intracloud lightning discharges and their associated radio emissions, J. Geophys. Res., 104, 4189–4212, 1999.

Smith, D. A., Eack, K. B., Harlin, J., Heavner, M. J., Jacobson, A. R., Massey, R. S., Shao, X. M., and Wiens, K. C.: The Los Alamos Sferic Array: A research tool for lightning investigations, 107, D13, doi:10.1029/2001JD000502, 2002.

Suszcynsky, D. M., Kirkland, M. W., Jacobson, A. R., Franz, R. C., Knox, S. O., Guillen, J. L. L., and Green, J. L.: FORTE observations of simultaneous VHF and optical emissions from

lightning: Basic Phenomenology, J. Geophys. Res., 105, 2191–2201, 2000.

Suszcynsky, D. M., Light, T. E., Davis, S., Kirkland, M. W., Green, J. L., and Guillen, J.: Coordinated Observations of Optical Lightning from Space using the FORTE Photodiode Detector and CCD Imager, J. Geophys. Res., 106, 17897–17906, 2001.

Tierney, H. E., Jacobson, A. R., Roussel-Dupré, R., and Beasley, W. H.: Transionospheric pulse pairs originating in marine, continental and coastal thunderstorms: Pulse energy ratios, Radio Sci., 37, 11-11 through 11-17, 2002.

Uman, M. A., McLain, D. K., and Krider, E. P.: The electromagnetic radiation from a finite antenna, Am. J. Phys., 43, 33–38, 1975.

Watson, S. S. and Marshall, T. C.: Current propagation model for a narrow bipolar pulse, Geophys. Res. Lett., 34, L04816, doi:10.1029/2006GL027426, 2007.

Willett, J. C., Bailey, J. C., and Krider, E. P.: A class of unusual lightning electric field waveforms with very strong high-frequency radiation, J. Geophys. Res., 94, 16255–16267, 1989.

Willett, J. C., Le Vine, D. M., and Idone, V. P.: Lightning return stroke current waveforms aloft from measured field change, current, and channel geometry, J. Geophys. Res., 113, D07305, doi:10.1029/2006JD008116, 2008.